Journal of
Applied Remote Sensing

RemoteSensing.SPIEDigitalLibrary.org

Remote-sensing application for facilitating land resource assessment and monitoring for utility-scale solar energy development

Yuki Hamada
Mark A. Grippo

SPIE.

Remote-sensing application for facilitating land resource assessment and monitoring for utility-scale solar energy development

Yuki Hamada* **and Mark A. Grippo**
Argonne National Laboratory, 9700 South Cass Avenue, Argonne, Illinois 60439, United States

Abstract. A monitoring plan that incorporates regional datasets and integrates cost-effective data collection methods is necessary to sustain the long-term environmental monitoring of utility-scale solar energy developments in expansive, environmentally sensitive desert regions. An image processing routine using very high spatial resolution (VHSR; i.e., 15 cm) multispectral imagery collected in November 2012 and January 2014 was developed to characterize ephemeral streams, vegetation, and land surfaces in the southwestern United States, where increased utility-scale solar development is anticipated. In addition to information about desert landscapes, the methodology integrates existing spectral indices and transformations (e.g., visible atmospherically resistant index and principal components); a new index called the erosion resistance index (ERI); and digital terrain and surface models, all of which were derived from a common VHSR image. The methodology identified fine-scale ephemeral streams at greater detail than does the National Hydrography Dataset, and it accurately estimated the distribution of vegetation and the fractional cover of various surface types. The ERI classified surface types that have a range of erosive potentials. The remote-sensing methodology could ultimately reduce uncertainty and monitoring costs for all stakeholders by providing a cost-effective monitoring approach that accurately characterizes the land resources at potential development sites. [DOI: 10.1117/1.JRS.9.097694]

Keywords: utility scale; solar energy development; environmental monitoring; very high resolution; spectral indices; desert regions.

Paper 15084SS received Jan. 29, 2015; accepted for publication May 26, 2015; published online Jun. 23, 2015; corrected Jun. 30, 2015.

1 Introduction

Currently, there is significant interest in developing utility-scale solar energy in the southwestern United States because of the high incoming solar radiation in the region. For example, the U.S. Department of the Interior, Bureau of Land Management (BLM), established 17 solar energy zones (SEZs) (i.e., areas of public lands prioritized for utility-scale solar energy development) across six states in the southwestern United States.[1] However, the nature and magnitude of the adverse cumulative impacts that could result from utility-scale solar technologies are not well-understood, particularly at the landscape scale.[2–4] Consequently, there is a need to develop comprehensive, long-term monitoring programs specific to solar energy development.[2]

The direct clearing of land at a project facility construction site could significantly affect the offsite land cover and surface hydrology. For example, because flash flooding is common in deserts, channels must be significantly modified to redirect water away from the facility's infrastructure. These modifications could alter the offsite surface hydrology by increasing flow and erosion in some ephemeral streams, while decreasing flow in other locations. These physical changes could, in turn, affect land cover, especially vegetation cover, which is largely determined by water availability. Similarly, solar facilities could reduce sand transport, which could alter dune migration and the distribution of dune-associated vegetation. Consequently, long-term monitoring

*Address all correspondence to: Yuki Hamada, E-mail: yhamada@anl.gov

of surface hydrology and land cover is needed to assess possible future impacts from solar energy development.

Long-term monitoring of utility-scale solar energy projects will assist public land managers in various ways, including helping them to (1) identify the actual direct, indirect, and cumulative impacts of a project and compare them with predicted environmental impacts in a timely manner; (2) evaluate the effectiveness of mitigation measures at the project site; and (3) evaluate the success of offsite compensatory mitigation projects. The resulting monitoring data can be integrated into an adaptive management framework that ensures development occurs in an environmentally responsible manner.

In recent years, the use of remote sensing for environmental monitoring has become widespread. It incorporates emergent platform and sensor technologies and advanced modeling and data management. For example, the BLM's Assessment, Inventory, and Monitoring (AIM) Program emphasizes the importance of using remote sensing, in addition to traditional field-based environmental monitoring methods, to meet the need to collect a significant amount of data across expansive and remote public lands.[5] BLM is developing a pilot long-term monitoring strategy (LTMS) for solar development in the Riverside East SEZ, located in Riverside County, California, that will make significant use of remotely sensed data.

There are unique challenges in applying remote sensing to desert environments. Desert landscapes are characterized by a scarcity of water, highly reflective soils, and sparse and less vigorous vegetation than that found in nonarid environments. This combination seems to violate fundamental assumptions on which remote sensing is based, including (1) spectral reflectance signals from elements on the ground are isolated from environmental and instrumental noise, (2) targets are spectrally separable from background, and (3) different target types have unique spectral signatures.[6,7] In addition, the surface characteristics found in desert regions, such as a subtle topographical gradient and limited exposure of soils, make existing data collection and processing tools (e.g., light detection and ranging, the soil stability index[8]) inadequate for reliably characterizing monitoring indicators in drylands. Therefore, there is a need to develop remote-sensing methods that are applicable to monitoring the unique environmental features in desert regions.

Sustainable and successful long-term monitoring methods will likely need to be able to cost-effectively collect information about multiple resource types or monitoring indicators.[9] To accurately characterize many of the resources, such as small plant canopies and narrow ephemeral stream channels, very fine-scale remotely sensed data (e.g., <50 cm resolution) will be needed. Collecting very high spatial resolution (VHSR) multispectral images with high overlaps between adjacent image frames has a great potential to meet these requirements for monitoring a large areal extent relatively inexpensively by (1) resolving fine-scale landscape features (e.g., shrub canopies and narrow ephemeral stream channels), (2) providing height information on the vegetation and microtopography via an aerial triangulation technique, and (3) overlaying multiple data types (e.g., spectral and height information) with precise spatial and temporal fidelity.

The goals of this project were to (1) identify remote-sensing metrics using VHSR remotely sensed imagery, which are correlated with monitoring indicators; and (2) develop cost-effective remote-sensing methods for detecting, identifying, and mapping land surface features and properties that are relevant for environmental monitoring. We focused on three key resource attributes: vegetation, surface hydrology, and soils (or surface). Specific objectives were to (1) examine how effective VHSR remote sensing and spectral information are in characterizing the distribution of vegetation and land-cover types in desert environments, (2) develop a remote-sensing methodology for mapping ephemeral stream networks in desert landscapes using VHSR multispectral imagery, and (3) explore the spectral reflectance of the VHSR images and develop a new spectral index that would indicate erosion risks in desert environments.

2 Materials and Methods

2.1 *Study Area*

The study area is in the Palo Verde Mesa in eastern Riverside County, California (Fig. 1). The area is a part of the Riverside East SEZ, the largest of the SEZs designated by the BLM.[1] The

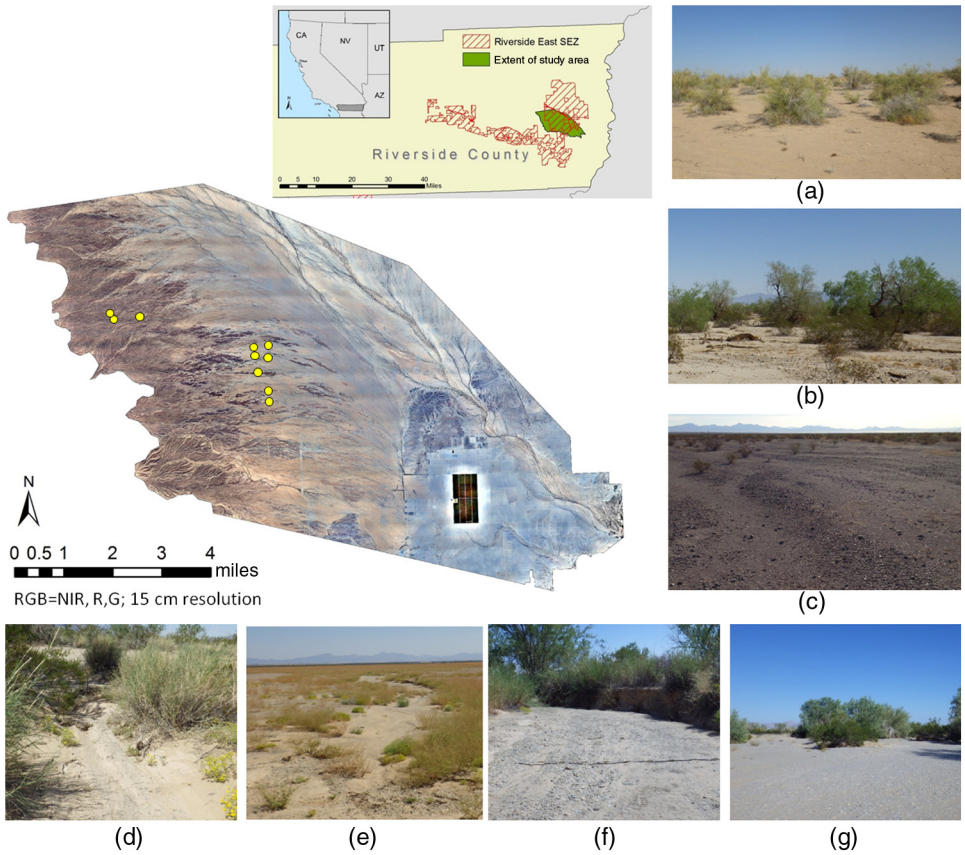

Fig. 1 Study area and typical landscape types: (a) desert scrubland, (b) riparian corridor, and (c) desert pavement. Ephemeral stream forms vary across (d) very narrow (<1 m wide) channels, (e) shallow, obscured channels, (f) a deep, well-defined, single channel, and (g) very wide (>200 m wide) multiple or braided channels.

total area designated for utility-scale solar energy projects within the SEZ is 598.6 km^2. As of April 2015, there were four authorized and three pending project applications located within or partially within the Riverside East SEZ; these projects cover an area of ~121 km^2, which equates to ~20% of the SEZ.

The study area extended ~170 km^2 for the 2012 data collection and 90 km^2 for the 2014 data collection. Both of these areas contain at least one solar energy project area. The area is covered primarily by bare ground, with sparsely distributed vegetation that consists of desert scrub species [e.g., creosotebush (*Larrea tridentata*), brittlebush (*Encelia farinose*), and white bursage (*Ambrosia dumosa*)]; microphyll trees [e.g., blue palo verde (*Parkinsonia florida*) and ironwood (*Olneya tesota*)]; and annual herbs such as desert sunflower (*Geraea canescens*). The area exhibits typical desert stream networks made up of single-thread and braided channels mixed with discontinuous forms. The ground surface consists primarily of loose, sandy soil; crusty soil; and desert pavement. Approximately a quarter of the area to the west exhibits rugged topography; it has ~130 m of elevation gain, from 185 to 315 m above mean sea level. The rest of the study area has a subtle topographic gradient towards the foothills. Solar facilities are typically sited in areas with minimal slope. Prior to facility construction, the site must be graded and cleared of vegetation.

2.2 *Data*

VHSR multispectral aerial images of the study area were collected on November 12 and 13, 2012, and January 15 and 16, 2014. The VHSR images consist of the blue, green, red, and near-infrared (NIR) spectral bands and have a 15 cm spatial resolution. Image frames have a forward image overlap of at least 50% and a side overlap of 60%. The image frames were

radiometrically corrected, mosaicked, orthorectified, and clipped to the study extent. Using the VHSR image frames, a digital surface model (DSM) and digital terrain model (DTM) were generated by the vendor, who used an automated aerial triangulation method. The DSM has a spatial resolution of 71.5 cm, and the DTM has one of 3.8 m.[10]

Field data were collected on September 25 and 26, 2012, and January 21–23, 2014. Occurrences of vegetation and bare ground (e.g., exposed soil and desert pavement) and plant life-form types were recorded.[10] Based on the information from the field survey, additional locations of vegetation, exposed soil, and desert pavement were manually digitized in the VHSR images in order to generate supplemental reference data for training and accuracy assessment. This image-interpretation approach was taken because the amount of data collected during the field work was restricted due to time constraints and inclement weather. At a 15 cm resolution, the VHSR images sufficiently resolved relatively small individual canopies in the scene, thereby supporting reliable identification of vegetation and other land surface features across the landscape.

2.3 *Image Processing*

Table 1 summarizes spectral vegetation indices (SVIs) that were examined for their effectiveness in characterizing monitoring indicators, such as vegetation distribution and cover, ephemeral streams, bare ground cover, and surface stability in the study area. The selected monitoring indicators were relatively amenable for remote sensing and were of interest in the Riverside East LTMS.

2.3.1 *Extracting vegetation features and estimating fractional cover*

A total of 10 SVIs that are widely used for vegetation studies (Table 1) were computed using the VHSR image mosaic. In the study area, nine small areas with known surface-type compositions were randomly selected, and their index values of vegetation were examined. The minimum

Table 1 Spectral vegetation indices.

Spectral vegetation indices	Definitions[a]	References
Normalized difference vegetation index (NDVI)	$(\rho_{NIR} - \rho_{red})/(\rho_{NIR} + \rho_{red})$	11
Green normalized difference vegetation index (GNDVI)	$(\rho_{NIR} - \rho_{green})/(\rho_{NIR} + \rho_{green})$	12
Visible atmospherically resistant index (VARI)	$(\rho_{NIR} - \rho_{green})/(\rho_{NIR} + \rho_{green} + \rho_{red})$	13
Ratio vegetation index (RVI)	ρ_{NIR}/ρ_{red}	14
Green–red ratio vegetation index (GRRVI)	ρ_{green}/ρ_{red}	15
Enhanced vegetation index (EVI)	$2.5 * [(\rho_{NIR} - \rho_{red})/(\rho_{NIR} + c_1 * \rho_{red} - c_2 * \rho_{blue} + L)]$ $c_1 = 6,\ c_2 = 7.5,\ L = 1$	16
Enhanced vegetation index 2 (EVI2)	$2.5 * [(\rho_{NIR} - \rho_{red})/(\rho_{NIR} + 2.4 * \rho_{red} + 1)]$	17
Soil-adjusted vegetation index (SAVI)	$(\rho_{NIR} - \rho_{red}) * (1 + L)/(\rho_{NIR} + \rho_{red} + L)$ $L = 0.5$	18
Modified soil-adjusted vegetation index (MSAVI)	$\left[2\rho_{NIR} + 1 - \sqrt{(2\rho_{NIR} + 1)^2 - 8(\rho_{NIR} - \rho_{red})}\right]/2$	19
Optimized soil-adjusted vegetation index (OSAVI)	$(\rho_{NIR} - \rho_{red})/(\rho_{NIR} + \rho_{red} + 0.16)$	20

[a] ρ_{blue}, ρ_{green}, ρ_{red}, and ρ_{NIR} are reflectance values of the blue, green, red, and near-infrared (NIR) spectral bands, respectively.

threshold value was interactively selected for each SVI layer to generate 10 vegetation maps. The accuracy of the vegetation maps was assessed using >2000 vegetation canopies and patches in three randomly selected areas that were independent from the previous nine areas, and the optimal SVI was selected.[10] The optimal SVI layer was combined with the original VHSR image mosaic, and iterative self-organizing classification[21] was performed to stratify the stacked image into 50 classes based on the similarity in pixel values across layers. Among the resultant 50 classes, five ecologically/environmentally meaningful and spatially cohesive classes (or surface types)—green vegetation, nonphotosynthetic vegetation (NPV), light-colored soil, dark-colored soil, and desert pavement—were identified based on the comparison with the VHSR image mosaic and field data. For each of the five surface types, training data were extracted from at least 10 groups of pixels. By using the training data, maximum likelihood classification was performed for the entire extent of the image in order to generate a preliminary surface type map.

A canopy height layer was generated by subtracting the DTM values from the DSM values. Height information was computed using only the 2014 data because the 2012 data were inadequate due to the insufficient overlap between frames during image collection. The height layer was overlain with the preliminary surface-type map, and the vegetation class was stratified into trees and shrubs. To produce a single bare ground class according to BLM's AIM Program criteria,[5] the light soil, dark soil, and desert pavement were merged. The final map delineated four surface types: trees, shrubs, NPV, and bare ground. The fractional cover of each surface type was computed for a 15 m × 15 m area using the surface-type map.[10]

2.3.2 *Extracting ephemeral streams*

An image-processing routine for extracting ephemeral streams was developed on the basis of landscape features associated with ephemeral channels that humans can recognize in the field and image. Channel beds that predominantly consist of loose, sandy soil, and fine-grained silt appear in a brighter color than the surrounding surface that contains a substantial amount of rock fragments. Ephemeral channels are often associated with riparian habitat characterized by dense, linear vegetation growth in the landscape. This simple association was translated into information about landscape features and structure that could be characterized in image processing using a series of spectral transformation and spatial statistical operations (Fig. 2).

To characterize desert vegetation, the modified, soil-adjusted vegetation index (MSAVI)[19] was first computed using the VHSR imagery. The minimum index value, 0.14 (−1.4 standard deviation from the mean), was interactively determined and applied to the MSAVI layer to map vegetation canopies and patches. Vegetation density was calculated by applying a 5-m-radius, circular, moving window to the vegetation map in order to identify riparian corridors and characteristic vegetation patterns along narrow channels. To characterize bright soil along channel beds, a principal component analysis was performed on the VHSR imagery. To characterize the local heterogeneity of brightness that resulted from the complex mixture of loose, erodible soils and adjacent vegetation, the local variability of the first principal component (PC1) layer, which exhibited the greatest brightness contrast, was calculated using a 1.5-m-radius area.

The two layers that represent vegetation density and spatial heterogeneity of surface brightness were combined to generate a single-layer stack. The statistical properties of vegetation density and brightness heterogeneity were extracted from ephemeral channel features and nonchannel features to obtain training data. Using these training data, maximum likelihood classification was performed on the layer stack to generate a preliminary ephemeral stream map. To fill holes and remove isolated fragments in the map, a morphological closing operation was applied to the preliminary map using a 1.5-m-radius moving window. A cluster of candidate channel pixels (with <30,000 pixels; ~675 m^2) was eliminated to exclude spatially incohesive pixels, and the final ephemeral channel classification map was generated. Channel centerlines were extracted from the raster classification map by identifying edges of Thiessen polygons that corresponded to channels, and irrelevant lines connecting to the centerline were removed to finalize the ephemeral stream centerline map.[10]

Both ephemeral channel classification and centerline maps were examined to evaluate how well the algorithm extracts stream channels in desert landscapes. The channel classification map

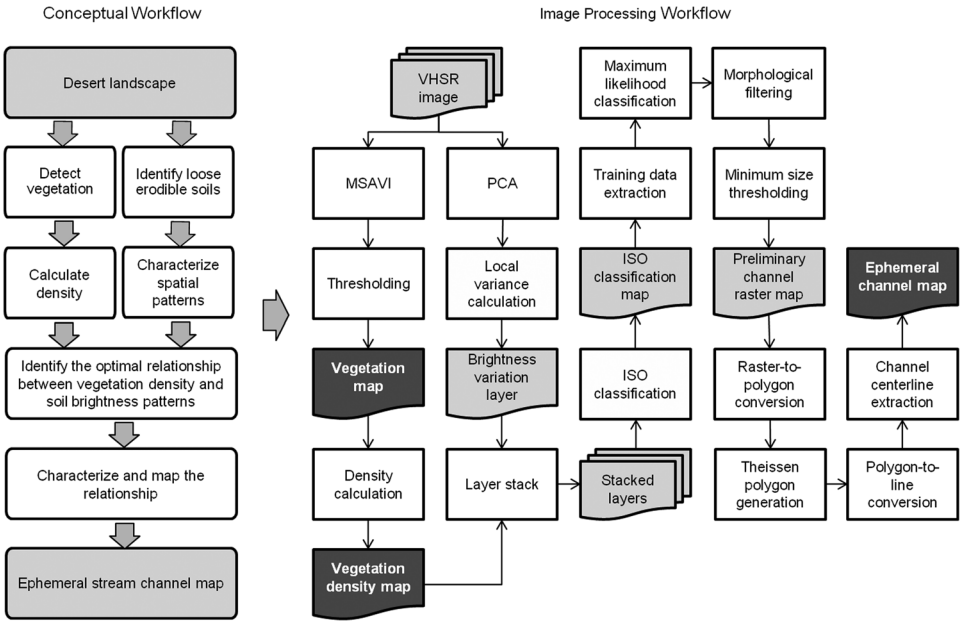

Fig. 2 Overview of the workflow for ephemeral stream channel extraction using very high spatial resolution multispectral image. The output and intermediate products that could inform land and resource management decisions are shown in dark and light gray, respectively. PCA, principal component analysis; VHSR, very high spatial resolution; MSAVI, modified soil-adjusted vegetation index; ISO, iterative self-organizing.

was first qualitatively examined with regard to the overall abundance and spatial patterns of the extracted channels by comparing it with the National Hydrography Dataset (NHD).[22] Quantitative analysis was performed using two 6-km^2 areas (or assessment areas). These assessment areas were selected from different parts of the study area to meet the goal of including various drainage types across the landscape. In each assessment area, 10,000 pixels that were located at least 1 m (7 pixels) away from each other were randomly selected. Pixels located within 1 m of channel boundaries were excluded from the assessment to compensate for uncertainty in the positional accuracy of reference polygon boundaries. The remaining validation pixels were used to compute accuracy metrics, including (1) the overall accuracy, (2) the producer's accuracy at indicating a false negative, and (3) the user's accuracy at indicating a false positive, as well as a kappa coefficient.

To evaluate the channel centerline map, the abundance and spatial distributions of channels were first qualitatively compared with the coarse-scale NHD to examine the level of detail represented by the aerial remote-sensing product. The local-scale accuracy of channel centerlines was evaluated based on the proportion of the channel centerline length that was extracted by our algorithm to the corresponding reference channel length. Delineation of 100% means that the extracted channel length equals the reference channel length and represents the highest accuracy. The analysis included all channel segments >150 m in both assessment areas. Next, the number of reference channels with $\geq 70\%$ and with $\geq 50\%$ of their channel delineated by the algorithm were identified and examined by independent analysts in order to determine whether the delineated channel centerlines could be visually recognized as channels, regardless of the proportion delineated. To minimize bias, the independent analysts were not involved in developing the algorithm or generating the reference data. This qualitative method was employed in order to gain an understanding of the spatial patterns of extracted channel segments.

2.3.3 *Developing the erosion resistance index for assessing surface stability*

Spectral reflectance values of the 2012 VHSR image set were extracted from 90 pixels that corresponded to six surface types: (1) streambeds mostly covered with loose, sandy soil,

and silt deposited by surface runoff; (2) unpaved roads dominated by sand that was mechanically disturbed by traffic; (3) desert scrublands; (4) bare ground containing noticeable gravel/rock fragments; (5) disturbed desert pavement; and (6) intact desert pavement. These surface types were expected to correspond to a gradient of surface stabilities ranging from low (streambeds) to high (desert pavement). Two-dimensional scatter plots were generated using all possible pairs of spectral bands and band ratios, and the combination that exhibited the greatest separability across the surface types was identified. A new index of surface stability—the erosion resistance index (ERI)—was derived by applying simple trigonometry to the spectral combination in order to identify the upper bounding line of the scatter plot, which corresponded to the most stable surface type. The perpendicular distance from the upper bounding line was calculated using the geometric equation developed by Perry and Lautenschlager:[23]

$$\mathrm{ERI} = \frac{\left(\left[b \times \frac{\rho_1}{\rho_2}\right] - \frac{\rho_3}{\rho_4} + a\right)}{\sqrt{b^2 + 1}}, \tag{1}$$

where a is the intercept of the upper bounding line and b is the slope of the upper bounding line. The values ρ_1 through ρ_4 are reflectance values of the VHSR imagery at given spectral bands. Pixels having greater ERI values indicate surfaces that would be more resistant to erosion and, thus, have a lower erosion risk.

Of all the scatter plots of possible pairs of spectral bands and band ratios using the 90 pixels corresponding to the six surface types, the plot of the green/red band ratio versus the green/NIR band ratio showed the best separation between the surface types (i.e., streambeds and unpaved roads, desert scrublands, bare ground with gravel, disturbed desert pavement, and intact desert pavement) (Fig. 3). The data space consisted of a lower bounding line corresponding to the surface type that is most resistant to erosion (e.g., desert pavements) and an upper bounding line representing the most erodible surface materials (e.g., streambeds and unpaved roads). Applying Eq. (1), the index was formulated as follows:

$$\mathrm{ERI} = \frac{\left[\left(-1.257 \times \frac{\rho_{\mathrm{green}}}{\rho_{\mathrm{red}}}\right) - \frac{\rho_{\mathrm{green}}}{\rho_{\mathrm{NIR}}} + 1.698\right]}{\sqrt{-1.257^2 + 1}}, \tag{2}$$

where ρ_{green}, ρ_{red}, and ρ_{NIR} are reflectance values of the green, red, and NIR spectral bands, respectively. Equation (2) was applied to the entire image, and the ERI was computed using both the 2012 and 2014 image sets. To evaluate the index, ERI values were extracted from areas of known surface types. A total of 189 pixels were sampled across the surface types. The ERI values were plotted by surface type, and summary statistics of the ERI values for each surface type were calculated. Box plots were generated to visualize overlap or separability between surface types.

3 Results

Results of mapping the three resource types—vegetation, surface hydrologic features, and land surface—are summarized in this section. Detailed results and analysis are discussed in Ref. 10.

3.1 *Vegetation Distribution and Fractional Land Cover*

Vegetation maps generated from SVIs indicated general vegetation locations correctly, with some exceptions (Fig. 4). For the riparian-scrubland transitional zone [Fig. 4(a)], NDVI, GNDVI, and VARI showed nearly identical detection patterns and tended to slightly overestimate vegetation. The rest of the SVIs tended to underestimate vegetation cover, particularly for shaded parts of canopies. In areas having vegetation over desert pavement, GNDVI, VARI, and RVI accurately detected vegetation. Pronounced overestimation was observed in the maps derived from NDVI and EVI.

Kappa values ranged from 0.69 to 0.88 and from 0.36 to 0.88 for the November 2012 and January 2014 image mosaics, respectively (Table 2). Most SVIs performed considerably better

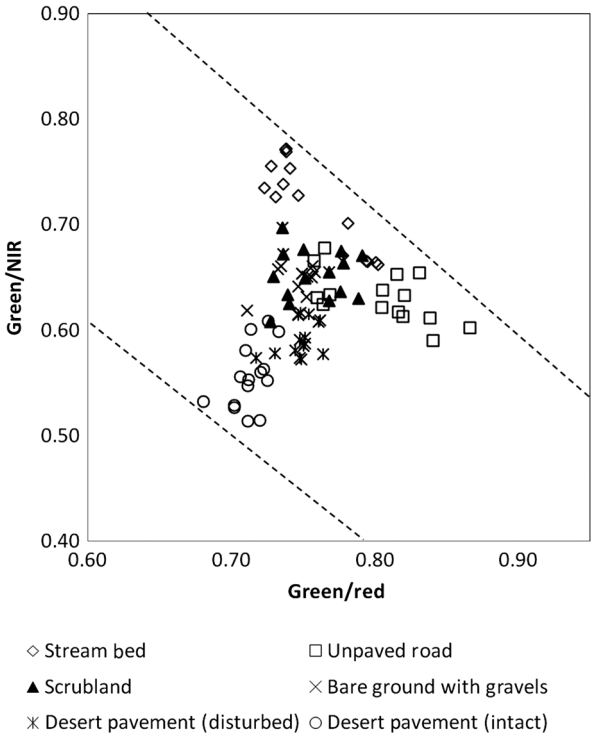

Fig. 3 Scatter plot of a green/red band ratio versus a green/NIR band ratio by surface type for correspondence to a range of erosion risks.

than random assignment; kappa values were $\gg$0.5 (exceptions were NDVI and EVI of the January 2014 product). In a comparison of the two image sets, the detection accuracy was higher in the November 2012 products (average kappa, 0.82) than in the January 2014 products (average kappa, 0.64). Regardless of the image set, SVIs often overestimated vegetation, as indicated by the false-positive rate being higher than the false-negative rate. Although a number of SVIs in the 2012 image clearly performed better than those in the 2014 image, VARI performed well for both image sets according to all three measures (kappa 0.875; false positive 15.0%; and false negative 12.2%, on average). VARI and GNDVI showed comparable performance, but VARI was superior to GNDVI because its accuracy between the two data collection dates was more consistent than that of GNDVI (e.g., for VARI, kappa 0.87 and 0.88; for GNDVI, kappa 0.69 and 0.87). In addition, the threshold values of VARI from the two datasets differed by only 0.02; this indicates that the index is stable for detecting vegetation in drylands as well as being robust in various environmental conditions in desert regions. On the basis of both these qualitative and quantitative assessments, VARI was selected for the fractional land cover calculation.

The fractional cover for the four surface types—tree, shrub, NPV, and bare ground—is shown in Fig. 5. Overall, bare ground was the dominant cover type in the study area, and the four surface types exhibited different abundance and spatial distributions across the landscape. Relatively high vegetation cover for both trees and shrubs formed linear features, and these features appear to follow along ephemeral streams in the study area (Fig. 5). Tree cover was greater along the McCoy Wash, extending from northwest to southeast in the eastern part of the study area. Dense shrub cover occurred in the western half of the landscape and along McCoy Wash.

The remote-sensing method estimated fractional cover accurately, with an error of <9% across nearly all plots, except for plot 7, which overestimated NPV and underestimated bare ground by 22.2 and 28.9%, respectively [Table 3(a)]. Overall error was considerably reduced by excluding plot 7 from the analysis. The mean error indicated a shift in the overall trend from positive (overestimation) to negative (underestimation) in the error for NPV estimation [Table 3(b)]. The mean absolute error and root-mean square error (RMSE) were ~2% lower for NPV and bare ground than those that occurred when plot 7 was excluded from the calculation, and the RMSE of bare ground noticeably dropped from 10.8 to 6.0% [Table 3(b)]. The

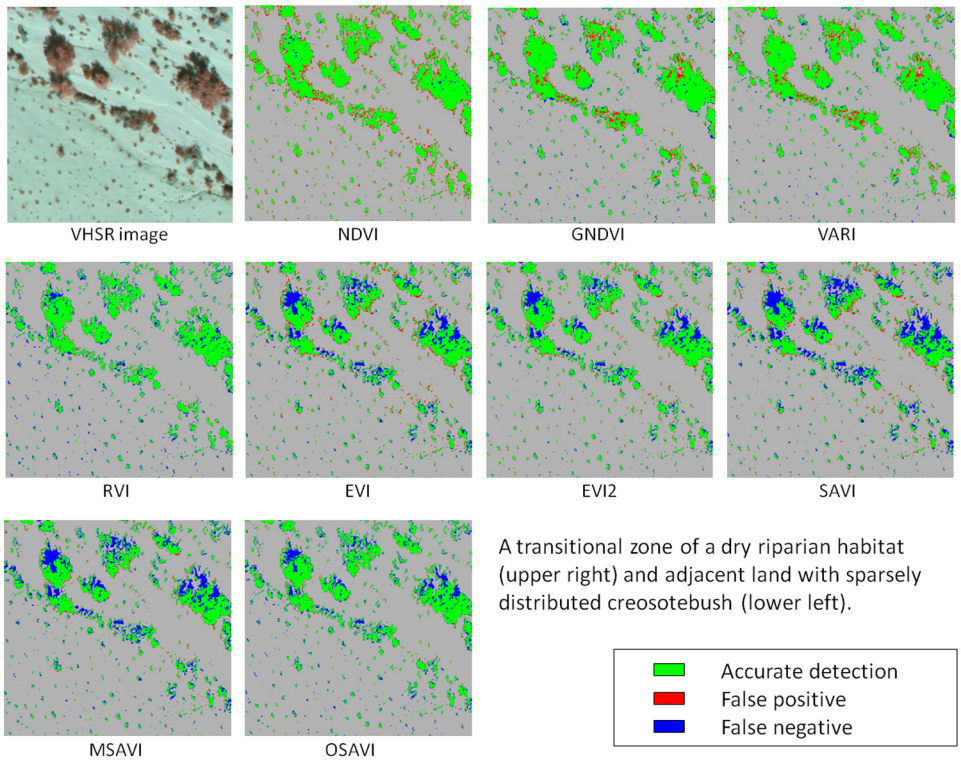

(a)

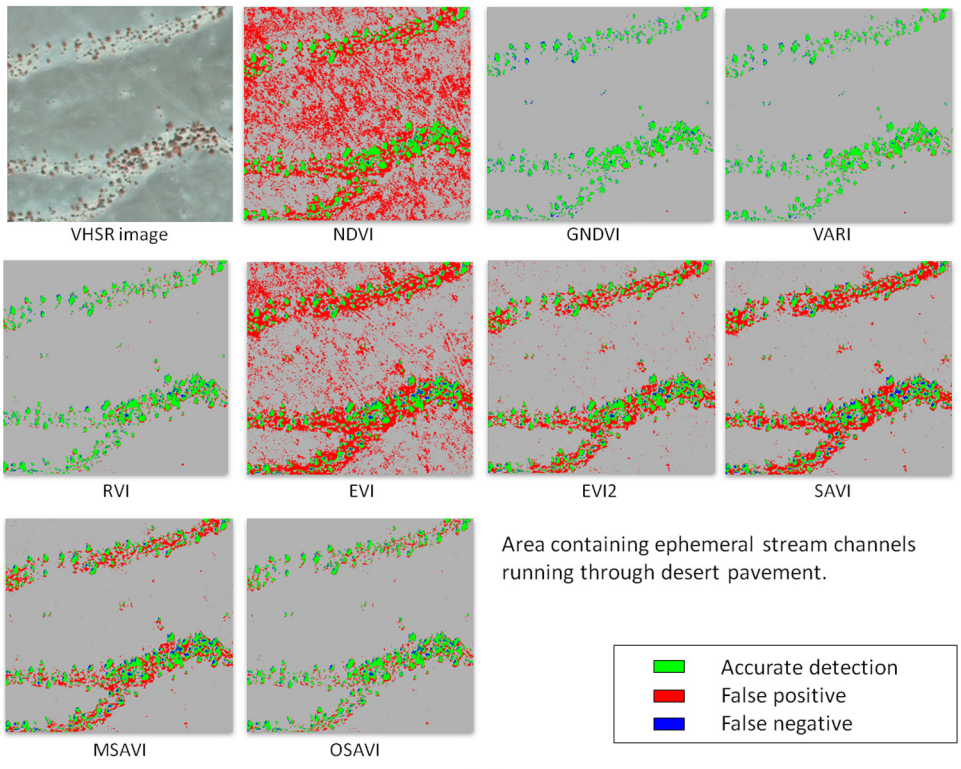

(b)

Fig. 4 Vegetation maps derived using spectral vegetation indices of the January 2014 image mosaic. The area shows a portion of (a) downstream riparian and (b) upstream ephemeral channel. VHSR, very high spatial resolution; NDVI, normalized difference vegetation index; GNDVI, green NDVI; RVI, ratio vegetation index; GRRVI, green–red RVI; EVI, enhanced vegetation index; SAVI, soil-adjusted vegetation index; MSAVI, modified SAVI; OSAVI, optimized SAVI.

Table 2 Accuracy of vegetation distribution.

Metric	NDVI	GNDVI	VARI	RVI	EVI	EVI2	SAVI	MSAVI	OSAVI
November 2012									
Threshold value	0.19	0.27	0.24	1.61	0.15	0.16	0.28	0.17	0.16
Kappa	0.85	0.69	0.87	0.78	0.78	0.88	0.84	0.87	0.87
False positive (%)	24.6	46.5	16.1	12.1	34.2	10.8	16.5	16.8	17.7
False negative (%)	3.5	1.0	14.1	14.3	4.2	13.5	15.4	9.0	6.6
January 2014									
Threshold value	0.13	0.34	0.23	1.45	0.11	0.11	0.22	0.12	0.13
Kappa	0.53	0.87	0.88	0.85	0.36	0.71	0.63	0.71	0.80
False positive (%)	63.1	14.1	14.0	9.5	70.8	34.5	41.1	28.8	16.1
False negative (%)	3.3	11.9	10.3	19.0	51.6	22.0	32.8	29.3	22.9

Note: NDVI, normalized difference vegetation index; GNDVI, green NDVI; RVI, ratio vegetation index; GRRVI, green–red RVI; EVI, enhanced vegetation index; SAVI, soil-adjusted vegetation index; MSAVI, modified SAVI; OSAVI, optimized SAVI.

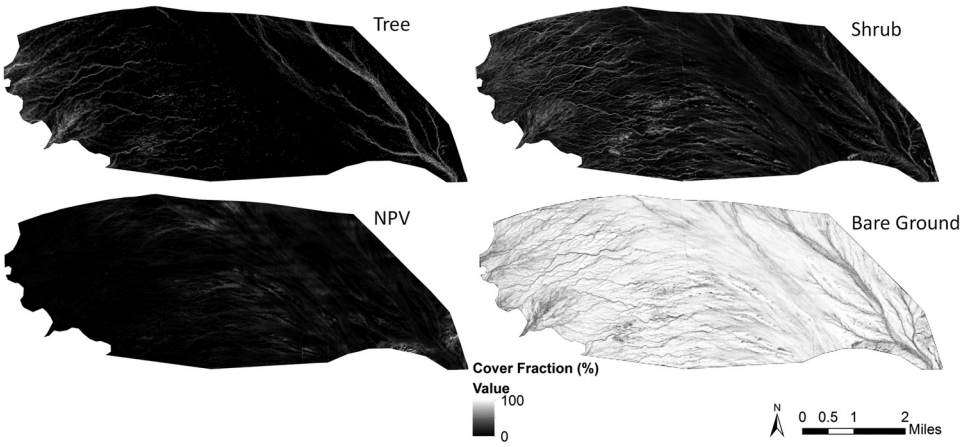

Fig. 5 Fractional cover maps of four surface types—tree, shrub, nonphotosynthetic vegetation (NPV), and bare ground—derived from the January 2014 image mosaic.

tree cover estimates were the most accurate of the four fractional cover estimates, while shrubs appeared to be slightly underestimated.

3.2 *Ephemeral Streams*

A considerable number of channel centerlines were delineated by the algorithm across the study area. The algorithm detected 900% more ephemeral streams than were mapped in the study area in the NHD developed by the U.S. Geological Survey (Fig. 6). Channel centerlines of McCoy Wash and other major tributaries were correctly delineated. Minor or narrow channels and those occurring in areas with even, sparse vegetation growth were frequently undetected by our algorithm. Channel features near stream headwaters were often missing from the final channel map. Although our algorithm correctly delineated wide channels consisting of well-defined braided forms, it had difficulty delineating wide channels with single-threaded forms when they were associated with heterogeneous vegetation growth along the channels.

Table 3 Accuracy of surface type fractional cover maps derived from remotely sensed image mosaic.

(a) Accuracy by plot

	Reference				Remote sensing estimate (RSE)				RSE – reference			
Plot	Tree (%)	Shrub (%)	NPV (%)	Bare (%)	Tree (%)	Shrub (%)	NPV (%)	Bare (%)	Tree (%)	Shrub (%)	NPV (%)	Bare (%)
1	3.1	12.5	12.5	71.9	2.5	7.6	15.4	72.1	–0.6	–4.9	2.9	0.2
2	4.7	12.5	20.3	62.5	5.0	7.9	16.9	67.9	0.3	–4.6	–3.4	5.4
3	7.8	3.1	9.4	79.7	3.3	5.0	4.9	85.6	–4.5	1.9	–4.5	5.9
4	0.0	10.9	4.7	84.4	0.1	6.6	3.3	88.2	0.1	–4.3	–1.4	3.8
5	0.0	10.9	9.4	79.7	0.0	8.0	2.9	86.3	0.0	–2.9	–6.5	6.6
6	0.0	14.1	6.3	79.7	0.0	9.5	3.2	86.2	0.0	–4.6	–3.1	6.5
7	0.0	3.1	10.9	85.9	0.0	7.8	33.1	57.0	0.0	4.7	22.2	–28.9
8	0.0	10.9	9.4	79.7	1.6	4.2	5.0	88.3	1.6	–6.7	–4.4	8.6
9	0.0	3.1	14.1	82.8	0.0	2.0	18.5	79.2	0.0	–1.1	4.4	–3.6
10	0.0	10.9	3.1	85.9	0.1	3.0	1.9	94.2	0.1	–7.9	–1.2	8.3

(b) Accuracy for all plots

	All plots				Excluding plot 7			
Error	Tree (%)	Shrub (%)	NPV (%)	Bare (%)	Tree (%)	Shrub (%)	NPV (%)	Bare (%)
ME	–0.3	–3.1	0.5	1.3	–0.3	–3.9	–1.9	4.6
MAE	0.7	4.4	5.4	7.8	0.8	4.3	3.5	5.4
RMSE	1.5	4.8	7.9	10.8	1.6	4.8	3.9	6.0

Note: NPV, nonphotosynthetic vegetation; ME, mean error; MAE, mean absolute error; RMSE, root-mean square error.

The difference between the channel length delineated by our algorithm and that present in the reference data varied between the two 6-km^2 assessment areas from the eastern and western portion of the study area (Table 4). The average difference in total channel length was 17.1%, with a range that went from 8.4% for the east area in the November 2012 data to 27.1% for the west area in the January 2014 data. When the ≥50% assessment criterion was applied, >60% of the reference channel segments were correctly delineated by our algorithm in both years, with one exception—the east area in the January 2014 data (Table 4). When the ≥70% assessment criterion was applied, slightly more than half of the reference segments were correctly delineated for the November 2012 data, but only about a third of the reference segments were delineated for the January 2014 data. A comparison of the west and east assessment areas by year revealed that the channel delineation accuracy for both areas for the 2012 data was nearly identical based on the ≥50% and ≥70% criteria. For the 2014 data, the delineation accuracy was comparable based on the ≥70% criterion; however, the accuracy for the west area was considerably higher than the accuracy for the east area when the ≥50% criterion was applied. In contrast to the modest accuracy of the criteria-based assessment, the independent analysts determined that >86% of the reference segments were correctly identified by our algorithm for each assessment area (Table 4).

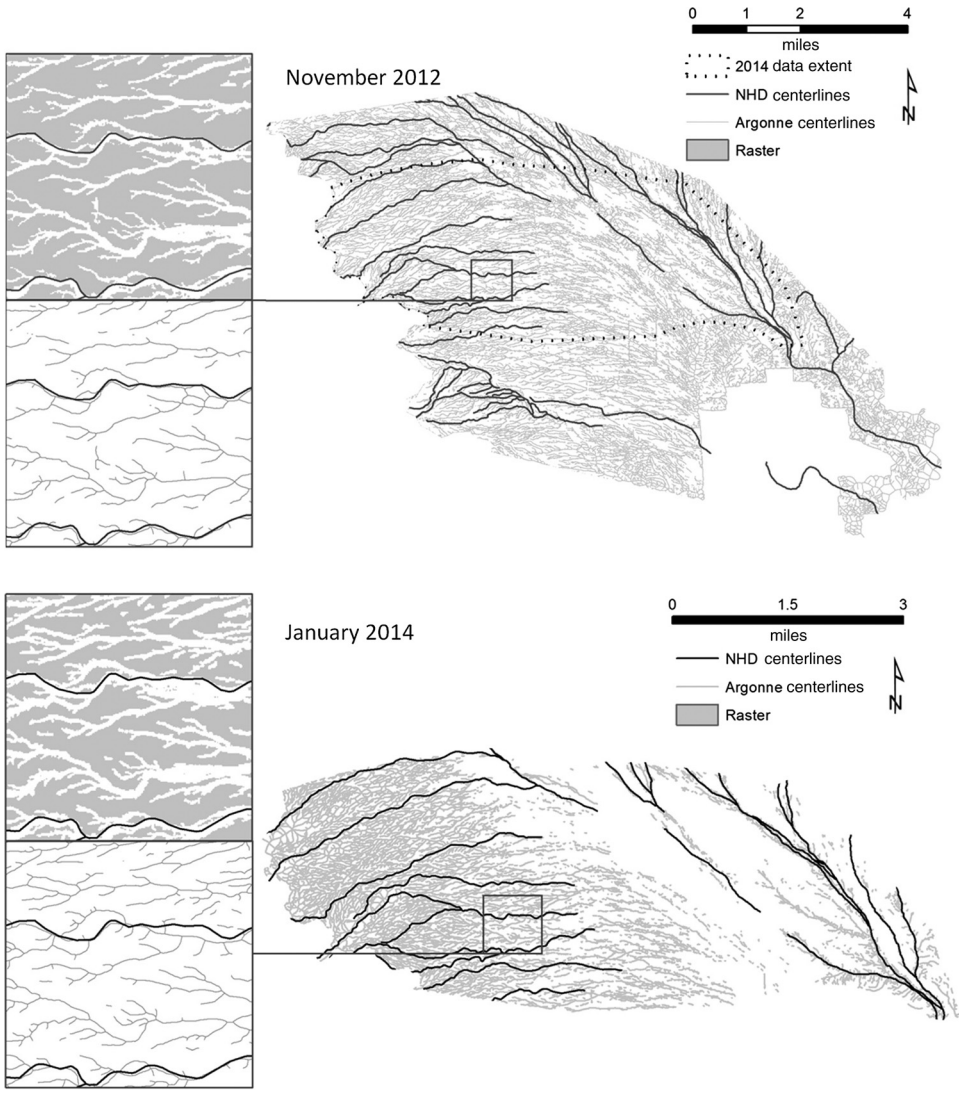

Fig. 6 Maps of ephemeral stream channels derived from the very high spatial resolution image overlain with the National Hydrography Dataset. McCoy Wash, which runs in a northwest-southeast direction, is visible running parallel to the northeast boundary of the study area. Argonne centerlines are channel centerlines extracted using our algorithm.

Table 4 Accuracy of ephemeral stream channel maps derived from remotely sensed image mosaic.

	November 2012[a]			January 2014[a]		
Length delineated	Pooled	West	East	Pooled	West	East
Total channel length (km)	146.0 (154.0)	50.9 (66.3)	95.1 (87.7)	79.5 (96.2)	51.6 (70.8)	27.9 (25.4)
Accurate delineation ≥70% (%)	56.3	53.0	59.5	38.1	38.6	37.5
Accurate delineation ≥50% (%)	66.5	65.5	67.5	60.9	84.2	37.5
Recognized (%)	89.0	86.0	92.0	87.4	89.5	87.5

[a]Values in parentheses indicate reference data.

3.3 *Surface Stability*

The ERI maps that were derived using Eq. (2) showed spatially cohesive distributions of relatively high and low ERI values across the study area (Fig. 7). Intact portions of desert pavement had high index values (warm colors: red, orange, and yellow), while surface materials mechanically disturbed by recreational vehicles appeared as linear features with lower index values (cool colors: magenta, purple, and blue) than those of the intact areas. The range of colors (e.g., from cool to warm) appeared to correspond to the severity of degradation from high to low sensitivity. Streambeds in large ephemeral washes—which, in the study area, often contain scattered shrub—showed extremely low index values (cool colors). As expected, shrub canopies (warm colors) were shown to have high resistance to erosion.

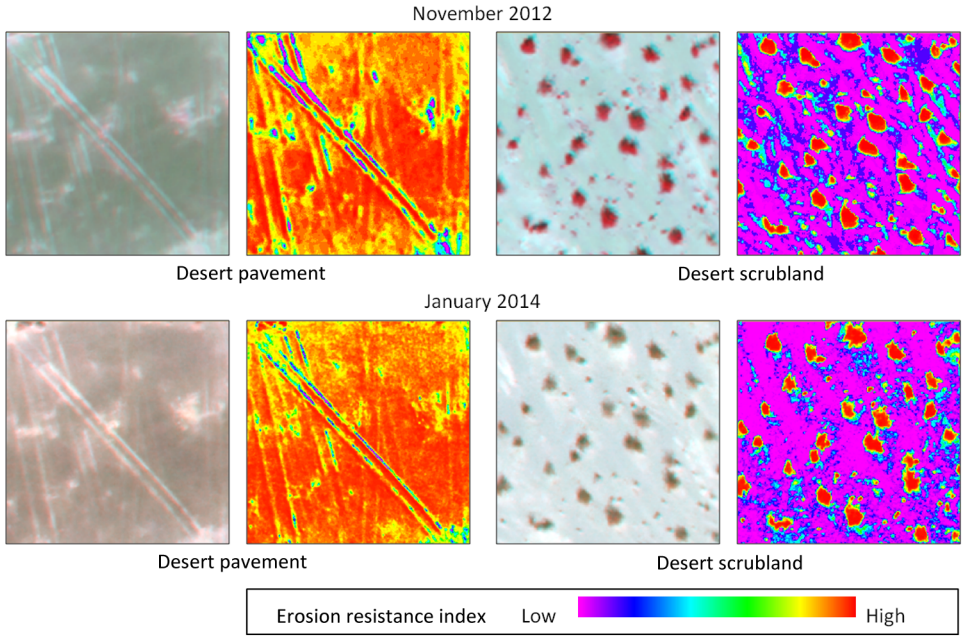

Fig. 7 Close-up views of VHSR images taken on November 2012 and January 2014 and erosion resistance index (ERI) maps of the corresponding areas.

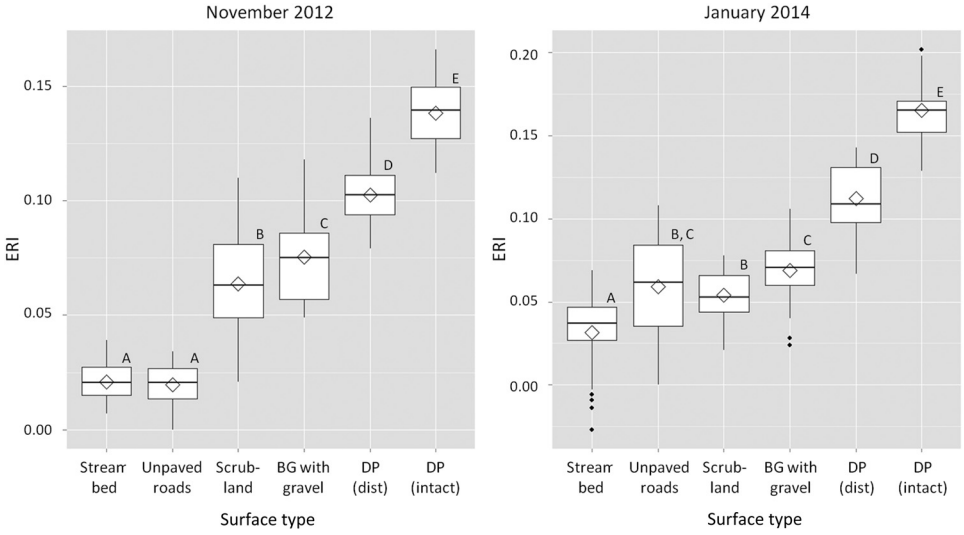

Fig. 8 Box plots of ERI by surface type from the November 2012 and January 2014 image mosaics. BG, bare ground; DP, desert pavement; dist, disturbed.

Box plots of ERI values from the 2012 and 2014 layers showed a trend of increasing index values from more erodible, sandy-soil-dominant surface types to more stable, rock-fragment-dominant surface types (Fig. 8). This trend suggests the index accurately characterized surface stability. However, some differences between the 2012 and 2014 results were apparent. In the 2012 ERI plot, the six surface types could be classified into four groups: (1) surface dominated by loose, sandy soil or fine-grained soil; (2) surface with noticeable nonsoil materials; (3) surface containing substantial rock fragments; and (4) surface completely covered by rock fragments. The first group is represented by streambeds and unpaved roads. The second group contains mixtures of soil, vegetation, and gravel. The third and fourth groups correspond to disturbed and undisturbed desert pavement, respectively. Pairwise t tests indicated no significant differences in the index values of streambeds and unpaved roads in 2012 (p is 0.64), while the ERI values for the rest of the surface types were significantly different from each other (p is <0.05). In contrast, in 2014, the difference in ERI values between streambeds and unpaved roads was statistically significant (p is 0.01), despite some overlap in index values. In addition, unpaved roads were indistinguishable from scrubland and bare ground containing substantial amounts of gravel. The two desert pavement surface types showed good separation from each other and from the other three surface types in both 2012 and 2014 (p of <0.05).

4 Discussion

VARI was not necessarily formulated to account for impacts from a bright soil background, but the index was the most accurate among the 10 SVIs examined. VARI also showed potential robustness with regard to environmental variability in desert regions because the difference of the threshold values between the two datasets was only 1% of its possible range (from −1 to 1). The MSAVI was selected to characterize riparian vegetation for ephemeral stream extraction because the extraction algorithm was developed prior to the vegetation study in order to meet the priority of the funding agency. MSAVI should be replaced with VARI for future analyses in order to improve the accuracy of extraction. Although extracted height values may not necessarily be precise (due to the insufficient number of reference features with a known height from which to generate tie points in the study area), the height information obtained from the image-based DTM and DSM was certainly effective for differentiating between trees and shrubs, which have similar spectral responses in drylands.

The considerably lower accuracy found in the fractional land cover of plot 7 than in those of the other plots is likely associated with its unique composition of land cover elements. Plot 7 was located in a large, less-defined wash that exhibited mixed ground color. A portion of the bare ground resembled dry plant litter or senesced herbaceous plants at the time of image collection. This spectral similarity likely resulted in the misclassification of bare ground as NPV. Differentiating NPV from background soil is often challenging when land cover in arid and semiarid environments is mapped using remotely sensed data.[24–26] The confusion between senesced herbaceous plants and bare ground may be alleviated by collecting imagery shortly after a rain event, when herbaceous plants are more photosynthetically active, such that herbaceous plants and bare ground would be spectrally separable. The increased greenness of the herbaceous plants could be problematic if differentiating between shrub and herbaceous vegetation is an important monitoring objective.

Bright-colored soil, dark-colored soil, and desert pavement were reliably differentiated using the VHSR images. These three bare ground types can be treated independently, although they were merged into a single class in this study. Desert pavement, in particular, is an ecologically significant cover type, and monitoring this resource would be useful for assessing surface disturbance and degradation from recreational activities or natural causes.

Most of the discrepancy in the number of ephemeral channels between the reference data and our product can be explained by the differences in how channels were defined in the two maps. For example, a wide tributary consisting of braided channels separated by a small distance was delineated as multiple channels in the reference data, but it was identified as a single broad channel by the algorithm. Surface patterns across desert scrublands that were created by unstructured surface sheet-flow may be defined as channels in the reference data but may not be

recognized as channels by the algorithm because they lack the typical characteristics of ephemeral channels. Establishing a common definition of ephemeral streams that is meaningful for ecological and management perspectives (e.g., active versus inactive, a single aggregated tributary versus a set of individual braided channels) is necessary in order to generate reliable reference data for assessing the accuracy of the map and appropriately refine the algorithm. Establishing a common definition of ephemeral streams and mapping their distributions would be useful for the local or landscape-scale hydrological modeling necessary to make resource management decisions.[27]

Differences in the accuracy of ephemeral steam detections between November 2012 and January 2014 (average kappa 0.82 and 0.64, respectively) probably stemmed partly from a landscape phenology that varied between the two dates. The difference in the accuracy of stream extraction data between the two time periods was more pronounced in the east area than in the west area. This might be due to edge effects that stemmed from the small amount of coverage in the 2014 image. The assessment area was defined based on the extent of the 2012 image. The 2014 image did not fully include the east assessment area because of the adjustments to and optimization of the image collection parameter done prior to the 2014 image collection. Although the accuracy calculation for the 2014 data was limited only to its image extent, the influence of potential edge effects was inevitable.

The higher stream extraction accuracy determined on the basis of the analyst-based assessment rather than the criteria-based assessment suggests that the channel segments extracted using the algorithm were spatially cohesive and formed linear configurations that showed a strong association with ephemeral stream channels present in the study area. This conclusion, in turn, suggests that including a pattern-recognition routine in the algorithm could further improve channel extraction accuracy as well as the effectiveness of the current algorithm.

ERI values were generally lower for the surface types that were expected to be unstable (e.g., streambeds and unpaved roads) and higher for the surface types that were expected to be more stable (e.g., desert pavement). However, the ERI did not consistently distinguish between similar surface types, which indicate that rigorous examination and refinement of the index are warranted. By mapping susceptibility to surface stability change, the ERI can be used to determine solar development avoidance areas and to identify areas where monitoring is a priority based on their high risk of erosion.

5 Conclusions

We developed a VHSR-based remote-sensing methodology that will support long-term, financially sustainable, environmental monitoring strategies for desert regions. This study demonstrated the utility of VHSR imagery to extract information about three land resource categories in a desert landscape—vegetation, surface hydrologic features, and land surface—within BLM-administered land designated for utility-scale solar energy development. Although further testing and refinement of the methodology are warranted before operational implementation, the methodology was found to be an effective means of extracting fine-scale information that would be valuable in understanding landscape features and their properties for multiple resource types at local or landscape scales. The cost-effective remote-sensing methods developed for this study can be integrated into environmental monitoring programs, such as the Riverside East SEZ's LTMS, thereby meeting the needs of authorizing agencies, developers, and stakeholders.

This study revealed that a few common spectral indices and transformations are useful for more than one type of resource and that output from a method for one resource type could serve as input for another resource type. For example, the vegetation distribution map was used not only to map the composition of vegetation (or fractional cover of surface types) but also to identify the distribution and abundance of riparian corridors for extracting ephemeral streams. In addition to assessing the resource types presented in this paper, we have examined the utility of remote-sensing methodology for assessing soil properties and biological soil crust distribution.[10] The results suggest that it is possible to extract information about multiple resource types from a single image source by integrating multiple, independent, image-processing algorithms

and methods into a single flow of work. The information extracted from VHSR images could complement information gathered from publicly available, high temporal frequency, coarse-resolution geospatial data and products (e.g., Landsat ETM+ imagery and MODIS products). In addition to the monitoring indicators examined in this study, the output from the remote-sensing methodologies could be used to study other resource types. For example, spectral indices and transformations that characterize vegetation density provide a basis for understanding the distribution and conditions of critical wildlife habitat in drylands. Thus, the remote-sensing methodologies developed in this study could potentially be applied to monitoring a broad range of plant and animal resources.

Acknowledgments

The authors thank Andrew Orr for developing the channel centerline extraction routine, Kelsey Wuthrich for generating the reference dataset for ephemeral stream channels, Scott Schlueter and Katie Rollins for participating in analyst-based accuracy assessment and Nicholas Haas for performing statistical analysis for Erosion Resistance Index. The authors also thank Ihor Hlohowskyj and anonymous reviewers for insightful comments on the manuscript. The submitted manuscript has been created by UChicago Argonne, LLC, Operator of Argonne National Laboratory ("Argonne"). Argonne, a DOE Office of Science laboratory, is operated under Contract No. DE-AC02-06CH11357. The U.S. Government retains for itself, and others acting on its behalf, a paid-up nonexclusive, irrevocable worldwide license in said article to reproduce, prepare derivative works, distribute copies to the public, and perform publicly and display publicly, by or on behalf of the Government. The project was funded by DOE's SunShot Initiative (#27239).

References

1. Bureau of Land Management and U.S. Department of Energy, "Final programmatic environmental impact statement (PEIS) for solar energy development in six southwestern states," FES 12-24, DOE/EIS-0403, Washington, DC (2012).
2. J. E. Lovich and J. R. Ennen, "Wildlife conservation and solar energy development in the desert southwest, United States," *BioScience* **61**(12), 982–992 (2011).
3. J. M. Northrup and G. Wittemyer, "Characterising the impacts of emerging energy development on wildlife, with an eye towards mitigation," *Ecol. Lett.* **16**(1), 112–125 (2013).
4. R. R. Hernandez et al., "Environmental impacts of utility-scale solar energy," *Renewable Sustainable Energy Rev.* **29**, 766–779 (2014).
5. G. R. Toevs et al., *Bureau of Land Management Assessment, Inventory, and Monitoring Strategy: For Integrated Renewable Resources Management*, Bureau of Land Management, National Operations Center, Denver, CO (2011).
6. M. A. Friedl, K. C. McGwire, and D. K. McIver, "An overview of uncertainty in optical remotely sensed data for ecological applications," Chapter 12 in *Spatial Uncertainty in Ecology*, G. T. Hunsker et al., Eds., pp. 258–283, Springer, New York, NY (2001).
7. D. Stow, "Monitoring ecosystem response to global change: multitemporal remote sensing analyses," Chapter 13 in *Global Change and Mediterranean-Type Ecosystems*, J. M. Moreno and W. C. Oechel, Eds., pp. 254–286, Springer, New York, NY (1995).
8. G. Pickup and D. J. Nelson, "Use of Landsat radiance parameters to distinguish soil erosion, stability, and deposition in arid Central Australia," *Remote Sens. Environ.* **16**(3), 195–209 (1984).
9. J. J. Taylor et al., "AIM-monitoring: a component of the BLM Assessment, Inventory, and Monitoring strategy," Technical Note 445, U.S. Department of the Interior, Bureau of Land Management, National Operations Center, Denver, CO (2014).
10. Y. Hamada, M. Grippo, and K. Smith, *Long-Term Monitoring of Utility-Scale Solar Energy Development and Application of Remote Sensing Technologies*, Argonne National Laboratory, Argonne, IL (2014).
11. C. J. Tucker, "Red and photographic infrared linear combinations for monitoring vegetation," *Remote Sens. Environ.* **8**, 127–150 (1979).

12. A. A. Gitelson, Y. J. Kaufman, and M. N. Merzlyak, "Use of a green channel in remote sensing of global vegetation from EOS-MODIS," *Remote Sens. Environ.* **58**(3), 289–298 (1996).
13. A. A. Gitelson et al., "Novel algorithms for remote estimation of vegetation fraction," *Remote Sens. Environ.* **80**(1), 76–78 (2002).
14. G. Birth and G. McVey, "Measuring the color of growing turf with reflectance spectrophotometer," *Agron. J.* **60**(6), 640–643 (1968).
15. G. L. Ritchie et al., "Sensitivities of normalized difference vegetation index and green/red ratio index to cotton ground cover fraction," *Crop Sci.* **50**(3), 1000–1010 (2010).
16. A. Huete et al., "Overview of the radiometric and biophysical performance of the MODIS vegetation indices," *Remote Sens. Environ.* **83**(1), 195–213 (2002).
17. Z. Jiang et al., "Development of a two-band enhanced vegetation index without a blue band," *Remote Sens. Environ.* **112**(10), 3833–3845 (2008).
18. A. R. Huete, "A soil-adjusted vegetation index (SAVI)," *Remote Sens. Environ.* **25**(3), 295–309 (1988).
19. J. Qi et al., "Modified soil adjusted vegetation index (MSAVI)," *Remote Sens. Environ.* **48**, 119–126 (1994).
20. G. Rondeaux and F. Baret, "Optimization of soil-induced vegetation indices," *Remote Sens. Environ.* **55**(2), 95–107 (1996).
21. J. T. Tou and R. C. Gonzalez, *Pattern Recognition Principles*, Addison-Wesley Publishing Company, Boston, MA (1974).
22. U.S. Geological Survey, *National Hydrography Dataset, 2009*, 18 June 2011, http://nhd.usgs.gov.
23. C. R. Perry and L. F. Lautenschlager, "Functional equivalence of spectral vegetation indices," *Remote Sens. Environ.* **14**(1), 169–182 (1984).
24. Y. Hamada, D. A. Stow, and D. A. Roberts, "Estimating life-form cover fractions within California sage scrub communities using remote sensing," *Remote Sens. Environ.* **115**(12), 3056–3068 (2011).
25. Y. Hamada et al., "Assessing and monitoring semi-arid shrublands using object-based image analysis and multiple endmember spectral mixture analysis," *Environ. Monit. Assess.* **185**(4), 3173–3190 (2013).
26. G. S. Okin et al., "Practical limits on hyperspectral vegetation discrimination in arid and semiarid environments," *Remote Sens. Environ.* **77**(2), 212–225 (2001).
27. M. Grippo, J. W. Hayse, and B. L. O'Connor, "Solar energy development and aquatic ecosystems in the Southwestern United States: potential impacts, mitigation, and research needs," *Environ. Manage.* **55**(1), 244–256 (2015).

Yuki Hamada is an assistant biophysical remote sensing scientist at Argonne National Laboratory. She received her BA and MS degrees in geography at San Diego State University and her PhD degree in geography from San Diego State University and the University of California Santa Barbara in 2010. Her research interests include optical data analysis for ecosystem function research and development of remote sensing methods for environmental monitoring, and remote sensing applications for subsurface ecosystem studies.

Mark A. Grippo is an ecologist at Argonne National Laboratory. He received his BA degree at the College of William and Mary, his MS degree in biology at Virginia Polytechnic Institute and State University, and his PhD degree in biology from Louisiana State University in 2009. His research interests include assessing the environmental impacts of energy development and developing tools to assess these impacts.